

# Stretchable High Response Piezoelectric Elastomers Based on Polable Polynorbornene Fillers in a Polydimethylsiloxane Matrix

Francis Owusu,\* Frank A. Nüesch, and Dorina M. Opris\*

To advance the field of piezoelectrics, it is desirable to find materials that combine high piezoelectricity with high elasticity. Applications such as self-sensors, stretchable electronics, soft robots, and energy harvesting would benefit tremendously. However, this is not an easy task neither for materials based on ceramics nor for those based on polymers. While ceramics can show strong piezoelectric effects, their mechanical response tends to be weak. Polymers instead are elastic but only few have sizeable piezoelectric effects. Additionally, they cannot maintain the polarization permanently as needed for piezoelectrics. Here, an all-organic piezoelectric elastomer is synthesized by blending high glass transition temperature ( $T_g = 104\text{ }^{\circ}\text{C}$ ) polar polynorbornene nanoparticles (NPs) with a high relaxation strength ( $\Delta\epsilon' = 22.4$ ) into a chemically cross-linked polydimethylsiloxane matrix. After processing the blends into thin films by doctor blading, they are poled by corona discharge at elevated temperatures. Fifteen days after poling, the materials show a stable and reversible piezoelectric response  $d_{31} = 37\text{ pC N}^{-1}$ . This, to the best of the authors' knowledge, not only is the highest  $d_{31}$  value reported, but the response is three times that of the well-known polyvinylidene difluoride.

piezoelectric properties. However, they exhibit drawbacks such as rigidity, brittleness, toxicity, high density, low breakdown field strength, and lack of design flexibility, limiting their extensive application in flexible and stretchable devices.<sup>[3–7]</sup> Although reported to show low piezoelectric properties compared to their ceramic counterparts, piezoelectric polymers are mechanically flexible, easier to process into complex designs, lightweight, cost-efficient, biocompatible, and possess large quasi-piezoelectric sensitivity.<sup>[8–10]</sup> There are numerous polymers reported to exhibit piezoelectric effects.<sup>[11–13]</sup> Among these, the well-investigated polyvinylidene fluoride (PVDF) and its copolymers with trifluoroethylene and tetrafluoroethylene represent the state-of-the-art in piezoelectric polymers. Besides, other polymers such as polyureas, polyamides, polyimides, polyesters, and polypeptides, to mention a few, have likewise been investigated

## 1. Introduction

Piezoelectric materials couple mechanical and electrical energy. Because of their excellent potential to generate electric charges in response to mechanical deformations, these smart materials have been widely investigated for self-powered sensors, actuators, and energy harvesting applications.<sup>[1,2]</sup> Ceramics materials such as the famous lead zirconate titanate (PZT) family dominate commercial applications due to their outstanding


for their piezoelectric response.<sup>[11]</sup> For instance, Takase et al. investigated the piezoelectric properties of nylon 7 and nylon 11. The recorded piezoelectric response, as a function of temperature, revealed maximal values of  $d_{31} = 17\text{ pC N}^{-1}$  for Nylon 7 and  $d_{31} = 14\text{ pC N}^{-1}$  for Nylon 11. However, moisture uptake issues impose limitations on their application in commercial devices.<sup>[14]</sup> Vinylidene cyanide and vinyl acetate copolymers have also been reported to give a piezoelectric response comparable to PVDF.<sup>[15]</sup> However, the synthesis of these copolymers is difficult and has hindered their development. Furthermore, an amorphous polyimide made of 2,6-bis(3-aminophenoxy) benzonitrile/4,4'-oxydiphthalic anhydride (( $\beta$ -CN)APB/ODPA), containing polar functional groups has demonstrated an impressive piezoelectric response for potential application at temperatures up to  $150\text{ }^{\circ}\text{C}$ .<sup>[13]</sup> However, most bulk piezoelectric polymers have a low mechanical strain at break and are not elastic, which hamper application in areas where large deformations are required.

Extensive research has shown that piezoelectric flexible materials can be achieved by design.<sup>[16–21]</sup> Ferroelectrets with a remarkable piezoelectric response have been reported using electrically polarized air-filled internal pores.<sup>[22–27]</sup> Their response was explained by R. Gerhard using a charge-spring model, which connects the piezoelectric coefficient with the elastic moduli of dipoles and matrix.<sup>[28]</sup> Matrices used include

F. Owusu, F. A. Nüesch, D. M. Opris  
Laboratory for Functional Polymers  
Swiss Federal Laboratories for Materials Science and Technology Empa  
Überlandstrasse 129, Dübendorf CH-8600, Switzerland  
E-mail: francis.owusu@empa.ch; dorina.opris@empa.ch

F. Owusu  
Institute of Chemical Sciences and Engineering  
Ecole Polytechnique Fédérale de Lausanne (EPFL)  
Station 6, Lausanne CH-1015, Switzerland

F. A. Nüesch  
Institute of Materials Science and Engineering  
Ecole Polytechnique Fédérale de Lausanne (EPFL)  
Station 6, Lausanne CH-1015, Switzerland

 The ORCID identification number(s) for the author(s) of this article can be found under <https://doi.org/10.1002/adfm.202207083>.

DOI: 10.1002/adfm.202207083

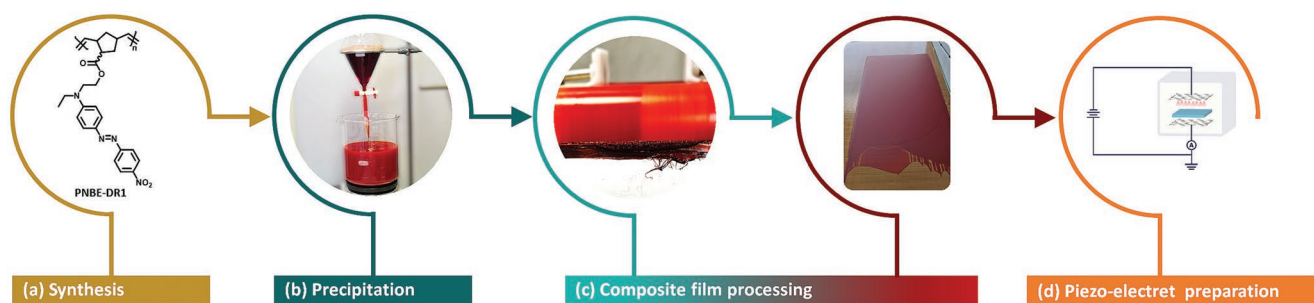


**Figure 1.** Process flow diagram showing techniques for preparing piezo-electret elastomer: a) synthesis of polar polymer; b) precipitation of polar polymer into a non-solvent; c) formation of homogenous composites using a three-roll-mill and processing it into thin films by Doctor Blading; and d) corona poling the films in a strong electric field at elevated temperatures.

polyolefins,<sup>[29,30]</sup> fluoropolymers,<sup>[31,32]</sup> cyclo-olefin polymers,<sup>[33]</sup> polycarbonates,<sup>[34]</sup> and polyesters.<sup>[35]</sup> The most extensively studied ferroelectret, cellular polypropylene (PP), has been used in flexible devices, including actuators, sensors, and generators.<sup>[36–38]</sup> While they exhibit excellent flexibility and large  $d_{33}$  piezoelectric response, these cellular materials' response strongly depends on their thermal processing and thermal history and they lack elasticity.<sup>[17,39]</sup>

Block copolymers with soft and hard blocks have also been explored, whereby the hard block served for charge trapping, and the soft block enabled elasticity.<sup>[40]</sup> Immobilizing polarized nanoparticles in a matrix of a dielectric elastomer enables the formation of stable stretchable electrets.<sup>[18,41,42]</sup> Piezoelectricity in such materials is introduced by poling in a strong electric field either by contact or corona poling.

In this work, we have prepared piezo-electret elastic materials with controlled structural and physicochemical properties using a composite approach in which a polydimethylsiloxane matrix is filled with polar high glass transition temperature ( $T_g$ ) polymer nanoparticles (Figure 1). Processing strategies have been adopted to make these materials into stretchable films with different morphologies to meet specific requirements for advanced technological applications. A permanent polarization, responsible for the piezoelectric effect, was introduced in the films by poling them in a strong electric field at temperatures above the  $T_g$  of the filler. Corona poling was used to minimize localized arcing during poling and to enable high poling fields without dielectric breakdown. The mechanical properties, dielectric behavior, remanent polarization, and piezoelectric responses were assessed as a function of time, frequency, and strain.

## 2. Results and Discussion

Two different stereoisomeric monomers of 5-norbornene-2-carboxylic acid (mixture of "endo" and "exo" with predominantly endo and pure exo) were successfully functionalized with *N*-ethyl-*N*-(2-hydroxyethyl)-4-(4-nitrophenylazo) aniline via Steglich esterification (Figure 1a; Scheme S1, Supporting Information) to give endo/exo mixture (M-A1) and purely exo – (M-A2) monomers. The synthesized polar monomers, known to exhibit a large dipole moment  $\mu$  of 10–12 Debye,<sup>[43]</sup> were successfully polymerized by ring-opening metathesis

polymerization (ROMP) under different conditions and using the same monomer to catalyst feed ratio. The two bulk polymers with regio-irregular structures were abbreviated as P-A1 (endo/exo mixture) and P-A2 (exo). The conversion rate for each polymerization was monitored over time by  $^1\text{H}$  NMR spectroscopy. Comparing the semi-logarithmic plot of  $[M_t]/[M_0]$  (where  $[M_0]$  represents the initial monomer concentration and  $[M_t]$  the concentration of monomer at a specific time) and the percentage conversion plot versus time for both monomers revealed different reaction rates for the respective polymers, P-A1 and P-A2. Detailed kinetic data for the polymerization can be found in Supporting Information (Figures S1–S4, Supporting Information). The final polymers were isolated in a yield of over 85% and thoroughly characterized (Figures S5–S9, Supporting Information).  $^1\text{H}$  and  $^{13}\text{C}$  NMR spectroscopy provided structural evidence of successful reaction and purification (Figures S5 and S6, Supporting Information). Gel permeation chromatography (GPC) elugrams in THF using polystyrene standard revealed monomodal molecular weight distribution for both polymers with number average molecular weights ( $M_n$ ) and polydispersity indices (PDI) as recorded in Table 1 (Figure S7, Supporting Information). Thermogravimetric analysis (TGA) was conducted to test the thermal stability and decomposition behavior (Figure S8, Supporting Information). Both polymers showed stability up to 168 °C before yielding to thermal decomposition. Differential scanning calorimetry (DSC) showed amorphous polymers (Figure S9, Supporting Information). The corresponding  $T_g$  values of the transitions are likewise listed in Table 1. The lowest  $T_g$  of 95 °C was measured for P-A2 and the highest of 104 °C for P-A1.

Polymer nanoparticles could be generated by displacing the solvent used in preparing polymer solutions with a nonsolvent, a method known as nanoprecipitation or "Ouzo effect,"

**Table 1.** Number average molecular weight  $M_n$ , polydispersity index (PDI), values of the glass transition  $T_g$ , decomposition temperature  $T_{d,1.5\%}$ , room temperature dielectric permittivity  $\epsilon'$ , and dielectric relaxation strength  $\Delta\epsilon$ .

Polymer ID	$M_n$ [Da]	PDI	$T_g$ [°C]	$T_{d,1.5\%}$ [°C]	$\epsilon'^a$	$\Delta\epsilon_{\text{max}}^b$
P-A1	275 000	1.30	104	168	4.3	19.5
P-A2	381 500	1.25	95	168	5.5	22.4

<sup>a</sup>Taken at 25 °C; <sup>b</sup>Taken at maximum relaxation.

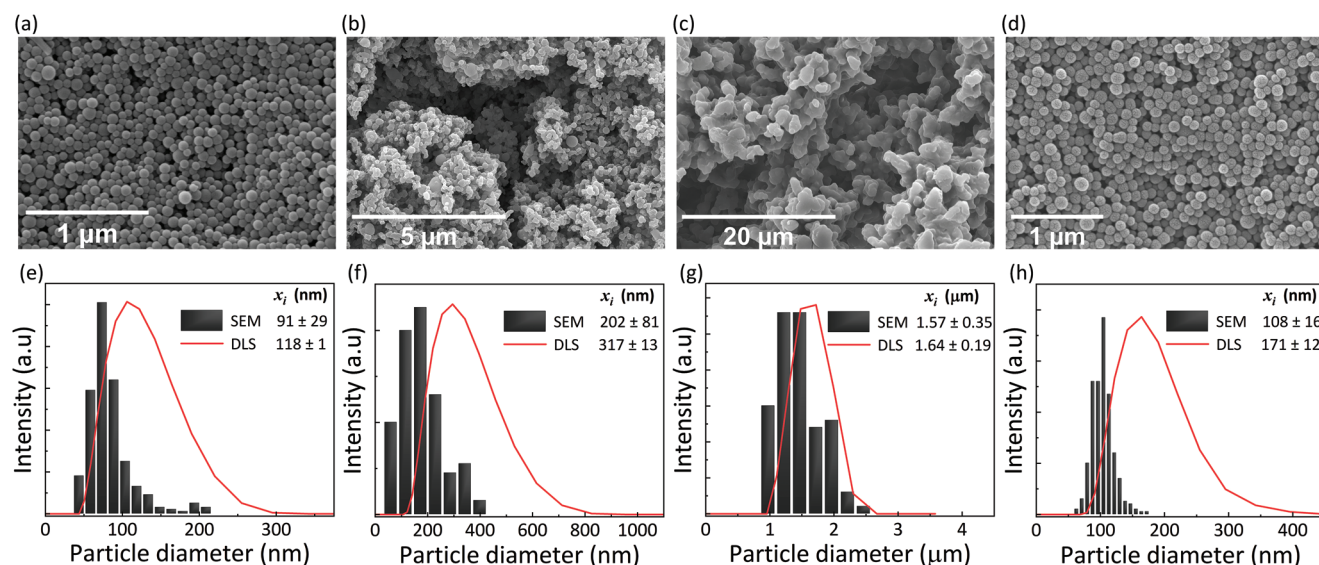


**Figure 2.** Representative SEM images and corresponding size-distributions obtained by SEM (black bars) and by DLS (red lines) made from **P-A1** concentration of: 2 g L<sup>-1</sup> (a,e); 5 g L<sup>-1</sup> (b,f); 10 g L<sup>-1</sup> (c,g); and **P-A2** concentration of 2 g L<sup>-1</sup> (d,h). Data are presented as mean ± SD (3 ≤ *n* ≤ 300) and *p* < 0.05.

as described in the Experimental Section. To avoid complex nonlinear influence on the particle size distribution as reported in the literature,<sup>[44,45]</sup> the ratio between solvent and nonsolvent for all preparations was kept constant at 0.33. A comparison is made for particles prepared from the initial polymer solutions of **P-A1** and **P-A2** in DCM with the same concentrations and by increasing the concentration for **P-A1** solutions. As expected, the same initial polymer concentration for **P-A1** and **P-A2** did not guarantee the same dynamics for the nanoprecipitation process, since the two polymers vary in *M<sub>n</sub>* (confirmed by GPC) and stereoregular configuration (elucidated by <sup>1</sup>H NMR). **Figure 2a,b,d,h** shows a slight variation in the mean sizes of the particles prepared from these two polymers with the same concentrations in DCM and the same solvent/nonsolvent ratio. Thus, the difference in their macromolecular coils in solution and hydrodynamic volumes affects the particle size. Furthermore, an increment in particle sizes was observed by varying initial polymer concentrations of **P-A1**. We observed that as the initial polymer concentration of **P-A1** was increased, the generated particles increased in size. Thus, increasing concentration leads to a high number of molecules per solvent volume, resulting in larger particle formation. The SEM micrographs and the corresponding size distributions determined by particle count using ImageJ and DLS analyses, as shown in **Figure 2**, reveal a pronounced dependence of particle size on the initial polymer concentrations. At concentration above 5 g L<sup>-1</sup>, the precipitated particles became more polydispersed and showed broader size distributions (**Figure 2b,c,f,g**).

A solution processing technique was employed to prepare composites of the polymer particles as filler in polydimethylsiloxane (PDMS) matrix. Processing steps and the solvent used are very crucial to obtaining composite films with good dispersion and excellent filler distribution in the matrix yielding desirable properties. For this reason, we employed a series of methods, including ball milling to break down large aggregates of polymer particles, homogeneous mixing of a well-dispersed

filler in matrix solution by shearing in a three-roll mill, and double-layer blade casting to minimize defects in the produced films. We successfully prepared composite films of **P-A1** and **P-A2** in PDMS solutions in cyclohexane with varying filler loadings and particle sizes. **Table 2** summarizes the amount and the size of the filler used as well as the elastic modulus at different strain levels of 5% (*Y*<sub>5%</sub>) and 50% (*Y*<sub>50%</sub>), storage modulus (*E'*), dielectric permittivity, and relaxation strength ( $\Delta\epsilon''$ ) of the materials synthesized. The obtained materials were denoted as **P-AX-Y-Z**, where **P-AX** represents the filler used, Y the size of the filler (small S, medium M, and large L), and Z represents the percentage weight (wt.%) of filler, respectively. Freestanding films with a typical thickness of 80 to 120 μm were achievable. The morphology of the produced films analyzed by SEM generally reveal evenly dispersed polymer particle fillers in the PDMS matrix. However, the extent of homogeneity and interfacial interaction between the two phases decreases with increasing filler particle size. The SEM micrographs in **Figure 3** provide evidence of phase separation as influenced by the particle size of the polymer filler. Again increasing filler content to 40 wt.% increases the chances of introducing micro-cracks as defects in the resultant films (**Figure S10**, Supporting Information).

Broadband dielectric spectroscopy (BDS) was employed to investigate the dipole relaxation dynamics in the polar polymers and the corresponding composites prepared. Thermally stimulated depolarization current (TSDC) as a complementary technique was also used to investigate the possibility of introducing quasi-permanent polarization in these amorphous materials. Graphical representations of how the real part  $\epsilon'$  and imaginary part  $\epsilon''$  of complex permittivity, the real part of the conductivity  $\sigma$ , and the loss tangent  $\tan \delta$  evolve with change in temperature at different frequencies for these materials can be found in the Supporting Information (**Figures S11–S15**, Supporting Information). The amount and size of filler have only a minor effect on the dielectric permittivity at room temperature, which is below 3, since the dipoles are frozen and cannot

**Table 2.** Summary of mechanical and dielectric properties of the prepared composites.

Mechanical Properties								
Composite	Filler <sup>a)</sup>	Filler particle size	Tensile DMA				Dielectric properties	
			$\gamma_{5\%}$ [MPa]	$\gamma_{50\%}$ [Mpa]	$E''_{1\%}$ [Mpa]	$E''_{10\%}$ [Mpa]	$\epsilon''^{b)}$	$\Delta\epsilon$
P-A1-S-10	10 wt.% of P-A <sub>1</sub> with a small particle size	91 nm	1.4	0.4	1.4	1.0	2.6	0.3
P-A1-S-20	20 wt.% of P-A <sub>1</sub> with a small particle size	91 nm	2.8	0.6	2.6	1.4	2.7	0.7
P-A1-S-30	30 wt.% of P-A <sub>1</sub> with a small particle size	91 nm	5.5	0.6	6.2	2.5	2.8	1.3
P-A <sub>1-M</sub> -30	30 wt.% of P-A <sub>1</sub> with a medium particle size	202 nm	5.1	0.7	6.7	2.5	2.7	1.2
P-A <sub>1-L</sub> -30	30 wt.% of P-A <sub>1</sub> with a large particle size	1.6 $\mu$ m	3.7	0.7	3.7	2.2	2.9	1.6
P-A <sub>2-S</sub> -30	30 wt.% of P-A <sub>2</sub> with a small particle size	108 nm	4.6	0.6	5.1	2.3	2.9	1.5
Matrix	–	–	0.6	0.2	0.5	0.5	2.4	–

<sup>a)</sup>In PDMS cross-linked networks; <sup>b)</sup>Taken at 25°C

be polarized. However, there is a noticeable increase in  $\epsilon'$  with increasing temperature above filler  $T_g$  over the specified frequency range. The experimental data were further interpreted by fitting with Havriliak–Negami (HN) relaxation model to understand the dielectric behavior with respect to structural and molecular motions of dipolar segments. A concise description of the dielectric behavior of such systems has already been given in another publication.<sup>[19,43]</sup> The parameters of relevance to understanding the temperature and frequency-dependent transitions taking place at the molecular level and the possibility of polarizing these materials are the dielectric relaxation time ( $\tau$ ) and the dielectric relaxation strength ( $\Delta\epsilon$ ). **Figure 4** provides information on the temperature-dependent behavior of the two dielectric relaxation parameters estimated from the

HN-fit function and the TSDC thermograms for the bulk polymers and their respective composites.

The two stereo-irregular polymers, P-A1 and P-A2, though possessing the same chemical composition, reveal a slight difference in their molecular dynamics in response to an electric field, attributed to variation in the structural configuration. Additionally, P-A1 and P-A2 have a relaxation strength of 19.5 and 22.4, which are higher than the values of 16.3 reported by our group on a poly(methyl methacrylate) modified with disperse red 1 moiety.<sup>[19]</sup> The higher value for the last indicates that this polymer should give a stronger piezoelectric response. The matrix environment significantly influences the relaxation time, delaying the reorientation motion of dipoles with an electric field. Additionally, the disparity in thermal expansion

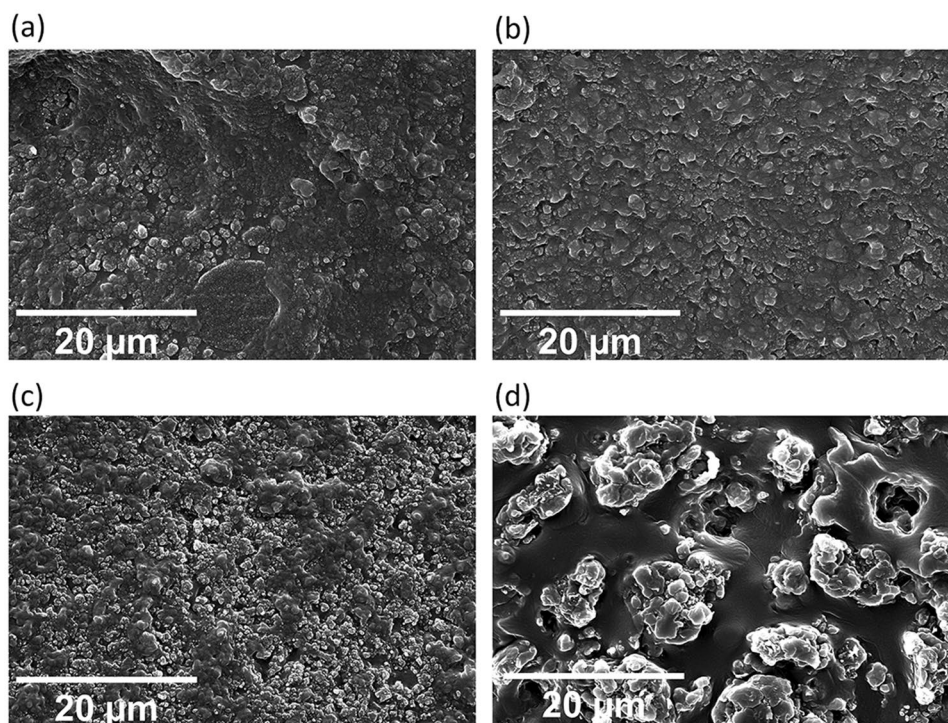


**Figure 3.** Effect of filler particle size on the morphology of prepared composites with 30 wt.% polymer particle loading in PDMS; a) P-A2-S-30; b) P-A1-S-30; c) P-A1-M-30; d) P-A1-L-30.

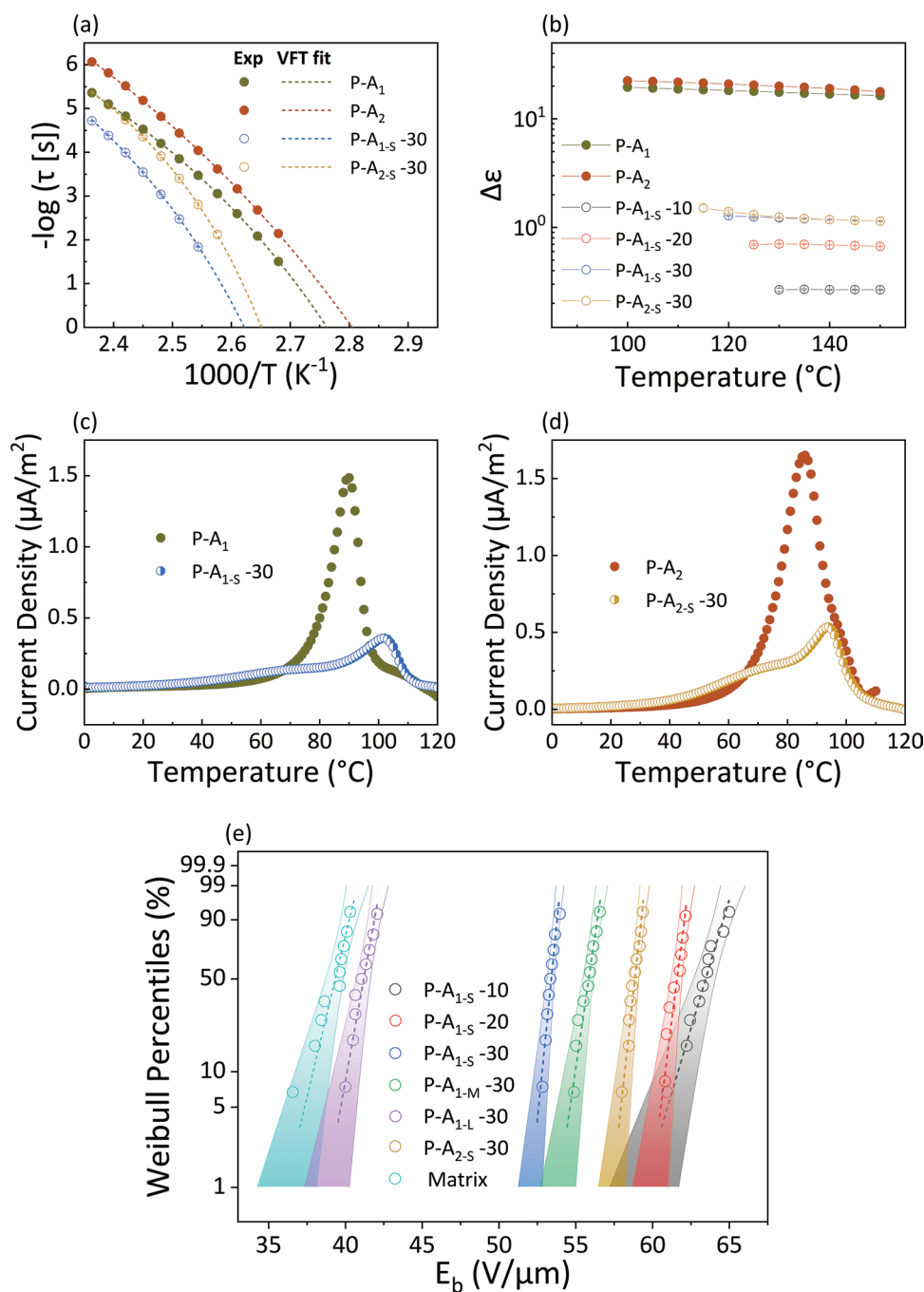


**Figure 4.** Dielectric behavior of P-A1 and P-A2, and their respective composites; a) Effect of matrix on the dynamics of  $\alpha$ -relaxation processes as shown in a Vogel–Fulcher–Tammann (VFT) plot corresponding relaxation times obtained from HN-fit versus the inverse of temperature; b) temperature dependence of dielectric relaxation strength; c) TSDC thermograms of P-A1 and P-A1-S-30; d) TSDC thermograms of P-A2 and P-A2-S-30, comparing temperature-dependent depolarization current density; e) Plot of dielectric breakdown of the composites in a two-parameter Weibull distribution and 95% confidence bands. Data are presented as mean  $\pm$  SD ( $3 \leq n \leq 10$ ) and  $p < 0.05$ .

coefficients and thermal conductivity of the polymer filler particles and PDMS matrix informs the resultant response in an electric field, as shown in Figure 4a. Interestingly, the relaxation behavior with respect to time ( $\tau$ ) was independent of the amount of filler (Figure S16, Supporting Information). The dielectric relaxation strength rather shows dependence on the amount of filler content and the stereoregular configuration

of the polar polymer particles, as plotted in Figure 4b. The complementary TSDC thermograms provided evidence of the various dipole contributions to polarization at very low frequencies and the possibility of poling the entire materials in a DC electric field. Detailed temperature-dependent poling and depolarization curves have been provided in supporting information (Figure S17, Supporting Information). Figure 4c,d shows that

the intensity of current density, which is also a contributing parameter to polarization, was higher in the bulk polar polymer than in their respective composites. The spike of these peak currents was observed close to the  $T_g$  of the respective polymers. As a confirmation of the matrix effect on the dielectric relaxation behavior of these polar polymers, we could observe peak shifts in the corresponding thermograms of their respective composites.

Dielectric breakdown measurements were statistically evaluated with a Weibull probability plot on several measured data sets. Figure 4e shows an increase in the dielectric breakdown field ( $E_b$ ) when the filler was added. This increase can be explained by the higher elastic modulus of the composites compared to the PDMS matrix. The increased breakdown field of the materials also confirms their high quality, since any film defect will lead to dielectric failure. However, a general decrease in  $E_b$  with increasing the amount of filler from 10 to 30 wt.% and the size of the filler particles was observed. Thus, the materials made with small particles performed best. The inferior performance of the materials made with larger particles is explained by the more inhomogeneous electric field in the material, which leads to earlier dielectric breakdown. A comparison between composites of the two stereo-irregular polymers with the same filler content of 30 wt.% and small particles shows different  $E_b$ . The elastic modulus of **P-A2-s-30** ( $Y''_{5\%} = 4.6$  MPa) is slightly lower than **P-A1-s-30** ( $Y''_{5\%} = 5.5$  MPa) and thus cannot explain the slight increase in  $E_b$  of the first. As will be discussed later, it seems that **P-A2-s-30** is more homogenous, which will lead to more homogenous distribution of the electric field in the material. However, it is still difficult to clarify where this difference comes from since the fillers have a different stereo-irregular structure and other extrinsic factors, such as film defects, can affect the  $E_b$ .

The mechanical properties of the prepared composites were evaluated using uniaxial tensile testing, cyclic deformations, and dynamic mechanical analysis (DMA), as provided in Supporting Information (Figures S18–S22, Supporting Information). All composites proved to be elastomeric, showing pronounced dependence of mechanical response on the composition of the material. Thus, the filler type, amount, and particle size affect the bulk mechanical behavior. Increasing the amount of filler led to an increase in Young's modulus and the strain at break. Keeping the filler content constant and increased particle size decreases Young's modulus and strain at break. The stereo-irregular polymer composites with the same amount of fillers gave similar tensile test results. The increase in Young's modulus with decreasing filler size and with increasing filler amount is explained by the increased cross-linking density due to the physical interactions between the polymer chains in the matrix and the filler. The improved tensile strength of all materials can be explained by the very good contact between the filler and the matrix, even though no compatibilizer was added. Polydimethylsiloxanes stick to most surfaces and are, therefore, often used as gluing agents. This strong adhesion may explain the improved mechanical properties of our materials. Cyclic deformation tests were also performed to further prove the mechanical integrity of these composites (Figure S19, Supporting Information). We generally observed an increase in stress softening under larger strain deformations (Mullins effect) with increasing the filler

content. Thus, materials lose stiffness after the first cycle, which is associated with the breakage of the interactions between the filler particles or filler and polymer chains.

DMA probed the viscoelastic behavior in the amplitude and frequency sweep modes (Figures S20 and S21, Supporting Information). A slight increase in the storage modulus and a slight decrease in  $\tan \delta$  with increasing frequency was observed for all materials except for the matrix. The loss factor  $\tan \delta$  gives valuable information regarding the non-elastic component in a material. The matrix–filler interface (interfacial region) strongly affects the mechanical properties of composites and quite often its damping level too. The  $\tan \delta$  of all materials was below 0.13 at all frequencies, which is rather low. An increase in  $\tan \delta$  with increasing the content of small particle filler content was observed, which indicates that the interaction between the matrix and the filler is less pronounced for the high filler content. Material **P-A2-s-30** has a smaller  $\tan \delta$  than **P-A1-s-30**, which may indicate a better interaction between the filler and the matrix for the first and may explain its increased dielectric breakdown field. However, for the materials with 30 wt.% filler, but different particles size, no clear trend was observed. Material made with medium size particles showed the highest  $\tan \delta$ . The reason behind this is unclear.

A strong dependence of the storage and loss moduli on strain amplitude with increasing filler content in composites was observed. This behavior is known as the Payne effect,<sup>[46,47]</sup> which is absent in the pristine PDMS matrix elastomer but strongly depends on the materials' filler content. At small strain amplitudes, the dynamic modulus is almost constant but decreases rapidly with increasing the strain. As expected, the storage modulus increases with the amount of filler and decreasing filler size. It is generally accepted that the dynamical break-up of filler networks is responsible for this nonlinear viscoelastic behavior of composite.

Storage modulus measurements were conducted at different temperatures from 50 to 150 °C (Figure S22, Supporting Information). Below the  $T_g$  of the filler, the materials showed an increase of the storage modulus at the rubbery plateau with the amount of filler and with decreasing particle size. This increase is due to filler–polymer and filler–filler interaction in the network structure. On increasing the temperature, a drop of storage modulus was observed for all samples, corresponding to the filler nanoparticles'  $T_g$ . These measurements also reveal an increasing dependence of the damping factor with increasing filler content and a decrease with increasing particle size.

Transverse piezoelectric coefficient measurements for the composites sets were conducted with an internally built technique. The testing setup, described in previous work in our lab, couples a Zwick Z010 tensile testing machine with a Keithley 2000 multimeter.<sup>[19]</sup> It allows applying a known force while straining the sample and recording the output electrical response (current and voltage) simultaneously. To affirm the reliability of these measurements, control samples of unpoled composites and poled matrix were studied alongside. An insignificant amount of current within the noise range of the measurement technique could be detected in all instances. This confirms that piezoelectric properties in the heterogeneous composite systems could only be induced after electric poling.

Samples of the composites were then subjected to thermally assisted corona poling to induce dipole alignment and anisotropic piezoelectric behavior in  $d_{31}$  mode. The procedure for poling is described in the Experimental Section. Directional changes in polarization experiments were also conducted by reversing the circuit connection to electrodes on the composite samples. This resulted in the flip of the direction of charge flow and a change in sign but a similar magnitude to the recorded current. The collected charge per cycle was calculated by integrating the recorded current. The piezoelectric coefficients and electromechanical coupling constants could then be calculated according to the equations provided in the Supporting Information. The resulting piezo-electrets after corona poling were tested for stability regarding their piezoelectric response over 1 month by applying 50% mechanical strain and measuring the output current and voltage. The evaluated piezoelectric properties generally experienced a non-exponential decay over 15 days characterized by a relatively strong decrease followed by a pseudo-stable state over the study period. To prove the reason behind the piezoelectric decay, a poled sample was tested after

letting it stand for 3 weeks. Its response was similar to the sample tested at predetermined periods, suggesting that charge migration in the soft PDMS matrix is responsible for the decay and not the rearrangement of the particles in the matrix. If the creep was responsible for the decay, the sample stressed at predetermined time intervals should show a stronger decay, which was not the case. Therefore, we concluded that the decay is not due to mechanical relaxation but rather electrical. The material consists of a soft matrix with a  $T_g$  significantly below room temperature, while the filler consists of hard particles with a high  $T_g$ . During poling at elevated temperatures, not only the dipoles from the filler particles are polarized, but ions are also moved in both the matrix and the filler. Ion relaxation is a slow process, that takes time, but the soft matrix facilitates the ion movement.

Figure 5a shows piezo-electrets of the stereoirregular polymer composites, which gave the highest performance. We further observed that piezoelectric properties were enhanced by increasing the active polar polymer filler content. That notwithstanding, the particle size of the filler plays a critical role; thus,

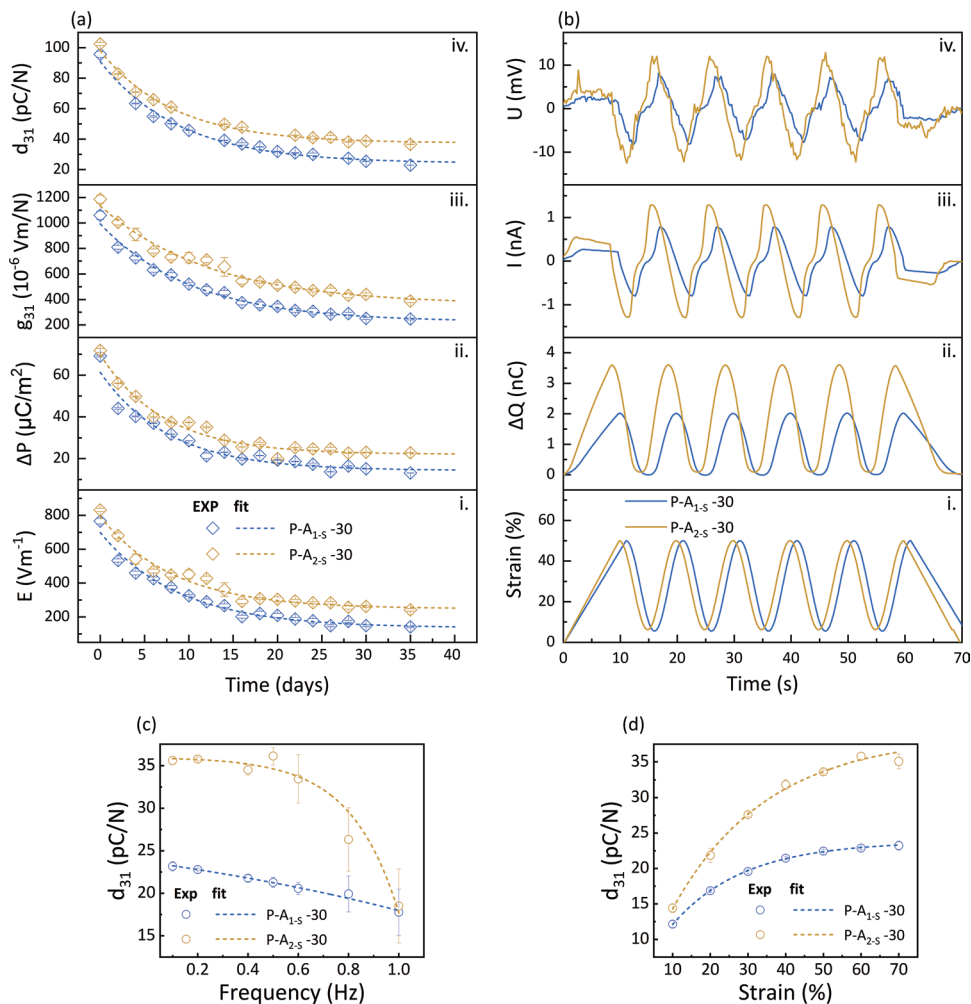


**Figure 5.** Piezoelectric response of P-A1-S-30 (blue) and P-A2-S-30 (yellow) elastomers: a) Non-exponential decay of charges collected at 50% strain deformation cycles over time; i) stress-induced electric field,  $E$ ; ii) stress-induced polarization,  $\Delta P$ ; iii) estimated transverse piezoelectric voltage coefficient,  $g_{31}$  and (iv) calculated transverse piezoelectric charge coefficient,  $d_{31}$ ; b) applied strain (i) generated charges (ii), current (iii), and voltage (iv); c) frequency dependent  $d_{31}$ ; and d) strain dependent  $d_{31}$  values. Data are presented as mean  $\pm$  SD ( $n = 15$ ) and  $p < 0.05$ .

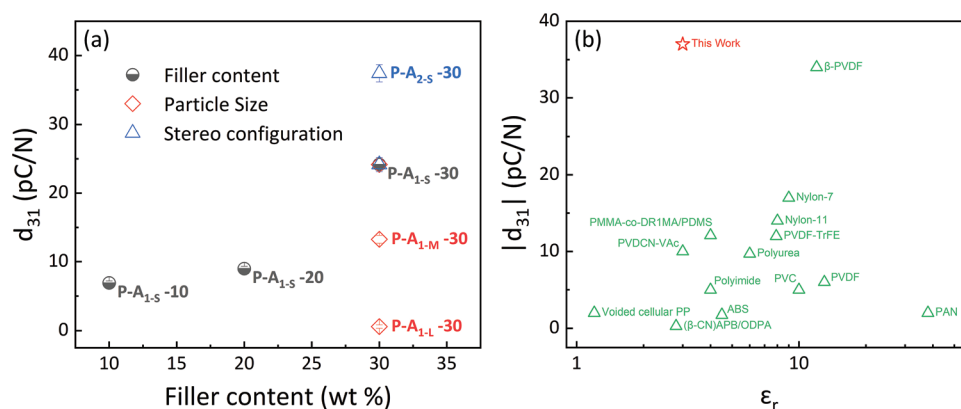


**Figure 6.** Summary: a) Effect of different amounts and filler sizes on the  $d_{31}$  and b) piezoelectric response of different piezoelectric polymers with different relative permittivity and of the best material developed in this work.

increasing filler particle size with the same content in composite resulted in a decrease in the piezoelectric response. The piezoelectric response is explained by the charge-spring model described by<sup>[28]</sup>:

$$d_{33} = \frac{-P_3}{Y_M} + \frac{P_3}{Y_D} \quad (1)$$

where  $P_3 = \epsilon_0 \Delta \epsilon(T) E_p$ ,  $Y_M$  is the Young's modulus of the matrix, and  $Y_D$  the Young's modulus of the filler (dipole phase). Our materials have stiff dipoles since the filler has a high  $T_g$  and thus an elastic modulus, which is several orders of magnitude higher than the elastic modulus of the matrix with a low  $T_g$ . Therefore, when the materials are stretched, the material's dipole density changes, leading to a current flow between the electrodes. The graphical proof of the above observations can be found in the supporting information (Figures S23 and S24, Supporting Information). Figure 5b provides a typical representation of the applied sinusoidal strain and the corresponding stress-induced charges, current, and voltage generated for P-A1-S-30 and P-A2-S-30.

To confirm the influence of poling approach on the resultant piezo-electret, we performed electrode contact poling of P-A1-S-30 film and evaluated the piezoelectric property. It was revealed that the corona poled samples showed a  $d_{31}$  approximately three times higher than the electrode contact poled counterpart (Figure S25, Supporting Information).

A summary of the transverse piezoelectric coefficient,  $d_{31}$ , as influenced by the filler content, particle size and stereoregular configuration of the different polar polymers for the prepared piezo-electret composites is shown in Figure 6a. Material P-A2-S-30 exhibited the highest  $d_{31}$  of 37 pC N<sup>-1</sup> at 50% strain, likely due to its larger relaxation strength. Its response is also three times larger than the one at 150% for a PDMS-based elastomer filled with poly(methyl methacrylate) modified dispersed red 1 poled by direct poling.<sup>[19]</sup>

Many flexible piezoelectric devices have an outstanding piezoelectric response when pressed, but are made of materials with high elastic modulus, which lack elasticity.<sup>[21,48–50]</sup> Aside the advantage of this material to withstanding comparatively large mechanical deformations, the recorded  $d_{31}$  value is comparatively the highest to already investigated polymers, as

presented in Figure 6b. Therefore, the material developed in this work may be suitable for applications where elasticity and compliance are a must, for instance, in implants.<sup>[51]</sup>

### 3. Conclusion

This work has employed suitable synthetic and composite preparation pathways coupled with electric poling to prepare piezo-electret elastomers. Polar norbornene monomers were first polymerized by ring-opening metathesis polymerization, and the resulting polymers were processed into nanoparticles via nanoprecipitation. Blends with different content and size of polar polynorbornene NPs in polydimethylsiloxanes were processed into thin films by doctor blading and the films were chemically cross-linked. To turn the materials piezoelectric, they were poled in a strong electric field above the  $T_g$  of the filler. The piezoelectric performance revealed a strong dependence on the amount, particle size, stereoregular configuration of the reinforced polymer NPs and the electric poling technique employed. Surprisingly, a quasi-stable transverse piezoelectric coefficient,  $d_{31}$ , as high as 37 pC N<sup>-1</sup> could be recorded for the best performing material poled by corona discharge. To the best of our knowledge, this is the highest value reported for elastic electrets. In addition, these piezo-electret elastomers can withstand large mechanical deformations, a critical property rendering them suitable for application in stretchable sensors, energy harvesting, soft robotics, and flexible electronics. Future work will be invested in increasing the piezoelectric response even further by introducing pores into the polarized films.

### 4. Experimental Section

**Materials:** All reagents were purchased from Sigma–Aldrich and utilized without further purification unless otherwise stated. Linear hydroxyl end-capped polydimethylsiloxane (PDMS) (AB116665,  $M_w = 139000$  g mol<sup>-1</sup>), ethyltriacetoxysilane crosslinker, and titanium 2-ethylhexoxide catalyst were purchased from ABCR. Dichloromethane (DCM), ethyl acetate, ethanol, methanol, heptane, cyclohexane, and tetrahydrofuran (THF) were purchased from VWR Chemicals and deuterated solvents from Deutero GmbH. DCM was dried over calcium hydride. Millipore Milli-Q system processed deionized water was

taken for all experimental work-ups. Polymers **P-A1** and **P-A2**, and their respective monomers were synthesized according to the literature with slight modification in reaction conditions.<sup>[43]</sup> A comprehensive overview of the syntheses with kinetic data of the polymerization can be found in Supporting Information (Figures S1–S4, Supporting Information).

**Preparation of Polymer Particles:** Particulate of the polymers **P-A1** and **P-A2**, with sizes in the nanometer to micrometer range, were prepared by solvent displacement technique. In practice, different polymer solutions (250 mL each) in DCM with concentrations of 5-, 8-, and 10 g L<sup>-1</sup> were prepared and separately added dropwise to 750 mL of methanol under vigorous stirring. The resulting polymer/DCM/methanol ternary systems were allowed to further stir for 30 min and the DCM carefully evaporated under vacuum. Subsequently, the colloidal suspensions were then filtered through a 0.22- $\mu$ m pore-size Nylon membrane and the obtained polymer particles were dried under vacuum at 25 °C. Polymer particles with an average size ranging from 100 nm to 2  $\mu$ m were achieved.

**Composite Film Processing:** Composite film, using the synthesized polymer particles as filler and PDMS as matrix components, was fabricated via solution processing coupled with blade casting. The filler was initially ball-milled using a Retsch MM 400 mixer mill (35 mL PTFE screw-top grinding jar and 1.25 mm diameter Zirconia grinding balls at 30 Hz for 30 min) to break down large aggregates and pre-dispersed in cyclohexane. The calculated amount of the matrix to give a set weight ratio of composition was added and manually mixed with a glass rod. Further mechanical agitation by shearing was performed on an EXAKT three roll mill with hard chromium-plated rollers (G-series) for 15 min to improve the homogeneity of the mixture. The resulting viscous slurry was further diluted with a small amount of cyclohexane (5 wt.% equivalence of the resulting viscous slurry) followed by the addition of ethyltriacetoxysilane crosslinker (100  $\mu$ L per gram of PDMS) and subjected to stirring overnight. Titanium 2-ethylhexoxide catalyst (10  $\mu$ L per gram of PDMS) was added and further stirred for 2–5 min. The resulting mixture was double-layer cast on Teflon coated glass substrate using a Zehntner ZUA 2000 blade. The produced film was first air-dried for 12–18 h to complete cross-linking reaction, followed by heat treatment in a vacuum oven at 100 °C for 8 h to remove residual solvent. Free-standing films with thicknesses ranging from 80 to 120  $\mu$ m could be processed.

**Structural Characterization:** <sup>1</sup>H and <sup>13</sup>C NMR spectra were recorded in CDCl<sub>3</sub> with a 400 MHz Bruker Avance-400 spectrometer at room temperature. The morphology of the synthesized polymer particles and composite films were characterized using FEI Quanta 650 ESEM. Images were taken in secondary electrons-topography mode using Everhart–Thornley Detector at 10 kV acceleration voltage. The particle size distribution in SEM images was evaluated by an average diameter count of  $\approx$ 300 particles. Dynamic light scattering (DLS) measurements were carried out on the particle suspensions produced after nanoprecipitation, using a Malvern Zetasizer at room temperature (25 °C). Measurements were conducted three times and always the average values were reported.

**Molecular Weight Determination:** Gel permeation chromatography (GPC) elugrams in THF were recorded with an Agilent 1260 Infinity, using two tandem-connected mixed-bed columns (1 $\times$  PL gel 5  $\mu$ m MIXED-C Guard and 2 $\times$  PL gel 5  $\mu$ m MIXED-C Analytical), coupled to a 390-MDS refractive index detector and calibrated with polystyrene standard. The system employed a flow rate of 1 mL min<sup>-1</sup> and was kept at 30 °C.

**Thermal Analysis:** Differential scanning calorimetry measurements were performed using a Perkin Elmer DSC 8000. Samples were initially heated to 150 °C at a rate of 20 °C min<sup>-1</sup> to remove any thermal history. Heat-cool-heat cycles were scanned from 0 to 150 °C at a rate of 20 °C min<sup>-1</sup> unless otherwise stated. Thermogravimetric analysis (TGA) was conducted using a Perkin Elmer TGA7 at a heating rate of 10 °C min<sup>-1</sup> under a nitrogen gas flow.

**Mechanical Behavior Evaluation:** Uniaxial tensile and repetitive cyclic deformation tests were performed on a Zwick Z010 universal testing machine with a 50- and 20 mm min<sup>-1</sup> crosshead speed. Dog-bone shape test specimens with gauge width of 2 mm and length of 18 mm were prepared by die-cutting. Reported data are averages of three independent measurements. The Young modulus was estimated from the slope of the

stress-strain curves using a linear fit to the data points within 10% strain. Dynamic mechanical analysis was carried out on an RSA 3 DMA from TA Instruments in the tensile mode. Stripes of samples with rectangular geometry were measured under a dynamic load of 4 g. Data in the frequency sweeps were obtained by applying 2% strain in the frequency range of 0.1–10 Hz. The amplitude scans were performed at 0.1 Hz from 1% to 10% strain. The temperature dependence measurements were conducted by applying 0.5% strain at a frequency of 0.1 Hz.

**Broadband Dielectric Spectroscopy:** Temperature-dependent dielectric properties were evaluated using a Novocontrol Alpha-A Frequency Analyzer equipped with quattro cryosystem temperature control. Samples of polymers **P-A1** and **P-A2** were prepared by making pellets with the aid of a hydraulic press, sandwiching them between two metal electrodes with 100  $\mu$ m glass fibres as spacers, and melt pressing at 120 °C. The composite films with known thickness were sandwiched between two metal electrodes. Dielectric spectra were recorded by applying an external electric field of 10 kV m<sup>-1</sup> in a frequency and temperature range of 0.1 to 1 MHz and –50 to 150 °C, respectively.

**Thermally Stimulated Depolarization Current Analysis:** A Novocontrol quattro cryosystem consisting of a cryostat with a sample holder coupled to a sensitive electrometer (B2985A, Keysight technologies) with a built-in dc voltage source was used for the measurements. Samples were prepared as described in the broadband dielectric spectroscopy procedure above. In practice, each sample was heated to a set polarization temperature ( $T_p$ ) and after stabilization, an electric field ( $E_p$ ) of 2 V  $\mu$ m<sup>-1</sup> was applied for a time ( $t_p$ ) of 1 min. The sample was steadily cooled at 10 °C min<sup>-1</sup> while keeping the electric field until the temperature reached 0 °C. The applied electric field was then removed. The sample was subsequently heated at 5 °C min<sup>-1</sup> after a delay time of 5 min. Currents accompanying the depolarization during this gradual heating process were recorded for analysis.

**Dielectric Breakdown Measurement:** A 12.5 kV dc high voltage power supply system (HCL 35–12500 pos, F.u.g electronic GmbH, Germany) was used for all measurements. Samples were sandwiched between two metal electrodes with 1 mm<sup>2</sup> area embedded in an epoxy resin. The applied voltage was linearly increased until failure voltage was recorded on several samples. Statistical analysis was employed to evaluate the dielectric breakdown field, commonly following Weibull probability model.

**Corona Poling:** Piezo-electret of the composite films were prepared by corona discharge in air atmosphere using a PolyK Technologies Corona poling system (PK-C30kV-200C). The system is equipped with a 30 kV/2 mA dc high voltage source, connected to a grid of corona needles mounted in an oven with digital temperature control. In practice, a specimen with a gauge width of 30 mm and a length of 60 mm is fixed on a poling frame and inserted into the poling station. The sample was then heated to a stabilized temperature of 120 °C, after which a voltage of 18 kV was applied to the grid of needles for 30 min. The poled film was then allowed to cool under the corona electric field for 30 min to room temperature. The voltage supply was finally switched off and the sample carefully unmounted.

**Electrode Contact Poling:** Specimen of the composites was sandwiched between two carbon black compliant electrodes circularly brushed on with 14 mm diameter. A maximum electric field of 25 V  $\mu$ m<sup>-1</sup>, beyond which the films yield electrical breakdown, could be applied at 120 °C for 10 min. The film was then allowed to cool to room temperature while keeping the electric field on at a rate of 10 °C min<sup>-1</sup>. The field was maintained by a Stanford Research Systems PS350 high voltage source. Temperature control was facilitated by a CTS-Temperature test chamber.

**Piezoelectric Coefficient ( $d_{31}$ ) Measurements:** Measurements were conducted on the same setup and following a similar procedure as described in the literature.<sup>[19]</sup>

**Statistical Analysis:** All data are evaluated by averaging several measurements without removing outliers ( $n \geq 3$ ). The data given in the manuscript represent the mean value, mean  $\pm$  standard deviation. Evaluation were performed employing descriptive statistics in the built-in functions of OriginLab. For image analysis, the built-in functions of ImageJ were used. A probability value ( $p \leq 0.05$ ) was significantly considered during analysis.

## Supporting Information

Supporting Information is available from the Wiley Online Library or from the author.

## Acknowledgements

This project has received funding from the Swiss National Science Foundation (IZSAZ2\_173358/1 and 206021\_150638/1), the Swiss Federal Laboratories for Materials Science and Technology (Empa, Dübendorf, Switzerland), and the European Research Council (ERC) under the European Union's Horizon 2020 Research and Innovation Programme (grant agreement No. 101001182). The authors acknowledge B. Fischer (Empa) for DSC, GPC, and TGA measurements, and Dr. D. Rentsch (Empa) for help with NMR measurements. The authors also acknowledge Prof. M. Negri (University of Buenos Aires, Argentina) for valuable discussions.

## Conflict of Interest

The authors declare no conflict of interest.

## Authors Contribution

D.M.O. initiated the work. F.O. did the synthesis, characterization, and analysis of data with support from D.M.O. The first version of the manuscript was written by F.O. with input from D.M.O. All authors contributed with discussions and approved the final version of the manuscript.

## Data Availability Statement

The data that support the findings of this study are available in the supplementary material of this article.

## Keywords

composite film processing, corona poling, elastic electrets, molecular dipoles, piezoelectric elastomers, piezoelectric polymers, transverse piezoelectric charge coefficient

Received: June 21, 2022

Revised: July 22, 2022

Published online: August 22, 2022

- [1] H. Yuan, T. Lei, Y. Qin, R. Yang, *Nano Energy* **2019**, 59, 84.
- [2] T. Mori, S. Priya, *MRS Bull.* **2018**, 43, 176.
- [3] V. L. Stuber, D. B. Deutz, J. Bennett, D. Cannel, D. M. de Leeuw, S. van der Zwaag, P. Groen, *Energy Technol.* **2019**, 7, 177.
- [4] S. Lee, Q. Shi, C. Lee, *APL Mater.* **2019**, 7, 031302.
- [5] C. Falconi, *Nano Energy* **2019**, 59, 730.
- [6] V. Jella, S. Ippili, J.-H. Eom, S. V. N. Pammi, J.-S. Jung, V.-D. Tran, V. H. Nguyen, A. Kirakosyan, S. Yun, D. Kim, M. R. Sihn, J. Choi, Y.-J. Kim, H.-J. Kim, S.-G. Yoon, *Nano Energy* **2019**, 57, 74.
- [7] Y. Liu, H. Wang, W. Zhao, M. Zhang, H. Qin, Y. Xie, *Sensors* **2018**, 18, 645.
- [8] S. Mishra, L. Unnikrishnan, S. K. Nayak, S. Mohanty, *Macromol. Mater. Eng.* **2019**, 304, 1800463.

- [9] M. Smith, S. Kar-Narayan, *Int. Mater. Rev.* **2022**, 67, 65.
- [10] N. Castro, N. Pereira, V. F. Cardoso, C. Ribeiro, S. Lanceros-Mendez, in *Frontiers of Nanoscience*, Vol. 14 (Eds: M. Benelmekki, A. Erbe), Elsevier, Amsterdam **2019**, p. 35.
- [11] Z. Ounaies, J. A. Young, J. S. Harrison, in *Field Responsive Polymers*, Vol. 726 (Eds: I. M. Khan, J. S. Harrison), American Chemical Society, Washington **1999**, p. 88.
- [12] J. S. Harrison, Z. Ounaies, in *Encyclopedia of Polymer Science and Technology*, John Wiley & Sons, Hoboken, NJ **2002**.
- [13] C. Park, Z. Ounaies, K. E. Wise, J. S. Harrison, *Polymer* **2004**, 45, 5417.
- [14] Y. Takase, J. W. Lee, J. I. Scheinbeim, B. A. Newman, *Macromolecules* **1991**, 24, 6644.
- [15] S. Miyata, M. Yoshikawa, S. Tasaka, M. Ko, *Polym. J.* **1980**, 12, 857.
- [16] A. H. Rahmati, S. Yang, S. Bauer, P. Sharma, *Soft Matter* **2019**, 15, 127.
- [17] R. Gerhard, in *Electromechanically Active Polymers: A Concise Reference* (Ed: F. Carpi), Springer, Cham **2016**, p. 489.
- [18] Y. S. Ko, F. A. Nüesch, D. Damjanovic, D. M. Opris, *Adv. Mater.* **2017**, 29, 1603813.
- [19] Y. S. Ko, F. A. Nüesch, D. M. Opris, *J. Mater. Chem. C* **2017**, 5, 1826.
- [20] K. Kapat, Q. T. H. Shubhra, M. Zhou, S. Leeuwenburgh, *Adv. Funct. Mater.* **2020**, 30, 1909045.
- [21] R. Ding, H. Liu, X. Zhang, J. Xiao, R. Kishor, H. Sun, B. Zhu, G. Chen, F. Gao, X. Feng, J. Chen, X. Chen, X. Sun, Y. Zheng, *Adv. Funct. Mater.* **2016**, 26, 7708.
- [22] X. Qiu, L. Holländer, W. Wirges, R. Gerhard, H. C. Basso, *J. Appl. Phys.* **2013**, 113, 224106.
- [23] S. Bauer, R. Gerhard-Multhaupt, G. M. Sessler, *Phys. Today* **2004**, 57, 37.
- [24] S. R. Anton, K. Farinholt, A. Erturk, *J. Intell. Mater. Syst. Struct.* **2014**, 25, 1681.
- [25] S. Gong, C. Wang, J. Zhang, C. Zhang, J. E. West, K. Ren, *Adv. Sustainable Syst.* **2018**, 2, 1700178.
- [26] A. Kachroudi, S. Basrour, L. Rufer, A. Sylvestre, F. Jomni, *Smart Mater. Struct.* **2016**, 25, 105027.
- [27] R. A. P. Altafim, X. Qiu, W. Wirges, R. Gerhard, R. A. C. Altafim, H. C. Basso, W. Jenninger, J. Wagner, *J. Appl. Phys.* **2009**, 106, 014106.
- [28] R. Gerhard, *Proc. SPIE* **2016**, 9798, 97980T.
- [29] M. Wegener, W. Wirges, J. Fohlmeister, B. Tiersch, R. Gerhard, *J. Phys. D: Appl. Phys.* **2004**, 37, 623.
- [30] M. Nakayama, Y. Uenaka, S. Kataoka, Y. Oda, K. Yamamoto, Y. Tajitsu, *Jpn. J. Appl. Phys.* **2009**, 48, 09KE05.
- [31] S. Zhukov, S. Fedosov, H. von Seggern, *J. Phys. D: Appl. Phys.* **2011**, 44, 105501.
- [32] P. Fang, F. Wang, W. Wirges, R. Gerhard, H. C. Basso, *Appl. Phys. A* **2011**, 103, 455.
- [33] Y. Li, C. Zeng, *Macromol. Chem. Phys.* **2013**, 214, 2733.
- [34] N. Behrendt, *IEEE Trans. Dielectr. Electr. Insul.* **2010**, 17, 1113.
- [35] W. Wirges, M. Wegener, O. Voronina, L. Zirkel, R. Gerhard, *Adv. Funct. Mater.* **2007**, 17, 324.
- [36] W. Li, D. Torres, T. Wang, C. Wang, N. Sepúlveda, *Nano Energy* **2016**, 30, 649.
- [37] N. Wu, X. Cheng, Q. Zhong, J. Zhong, W. Li, B. Wang, B. Hu, J. Zhou, *Adv. Funct. Mater.* **2015**, 25, 4788.
- [38] K. Kirjavainen, *US Patent* 4 654 546, **1987**.
- [39] Y. Zhang, C. R. Bowen, S. K. Ghosh, D. Mandal, H. Khanbareh, M. Arafat, C. Wan, *Nano Energy* **2019**, 57, 118.
- [40] C.-C. Hung, S. Nakahira, Y.-C. Chiu, T. Isono, H.-C. Wu, K. Watanabe, Y.-C. Chiang, S. Takashima, R. Borsali, S.-H. Tung, T. Satoh, W.-C. Chen, *Macromolecules* **2018**, 51, 4966.
- [41] S. Zhang, Y. Wang, X. Yao, P. Le Floch, X. Yang, J. Liu, Z. Suo, *Nano Lett.* **2020**, 20, 4580.
- [42] J. E. Q. Quinsaat, T. de Wild, F. A. Nüesch, D. Damjanovic, R. Krämer, G. Schürch, D. Häfliger, F. Clemens, T. Sebastian,

- M. Dascalu, D. M. Opris, *Composites, Part B* **2020**, 198, 108211.
- [43] F. Owusu, M. Tress, F. A. Nüesch, S. Lehner, D. M. Opris, *Mater. Adv.* **2022**, 3, 998.
- [44] S. Stainmesse, A. M. Orecchioni, E. Nakache, F. Puisieux, H. Fessi, *Colloid Pol. Sci.* **1995**, 273, 505.
- [45] I. Y. Perevyazko, J. T. Delaney, A. Vollrath, G. M. Pavlov, S. Schubert, U. S. Schubert, *Soft Matter* **2011**, 7, 5030.
- [46] K. Song, in *Progress in Rubber Nanocomposites* (Eds: S. Thomas, H. J. Maria), Woodhead Publishing, Sawston, UK **2017**, p. 115.
- [47] M. Shamonin, E. Y. Kramarenko, in *Novel Magnetic Nanostructures* (Eds: N. Domracheva, M. Caporali, E. Rentschler), Elsevier, Amsterdam **2018**, p. 221.
- [48] F. R. Fan, W. Tang, Z. L. Wang, *Adv. Mater.* **2016**, 28, 4283.
- [49] N. Wang, R. Daniels, L. Connelly, M. Sotzing, C. Wu, R. Gerhard, G. A. Sotzing, Y. Cao, *Small* **2021**, 17, 2103161.
- [50] T. Vijayakanth, D. J. Liptrot, E. Gazit, R. Boomishankar, C. R. Bowen, *Adv. Funct. Mater.* **2022**, 32, 2109492.
- [51] V. Jarkov, S. J. Allan, C. Bowen, H. Khanbareh, *Int. Mater. Rev.* **2021**, <https://doi.org/10.1002/09506608.2021.1988194>.